iScience

CellPress
OPEN ACCESS

Article

Synthesis and stability of switchable CO_2-responsive foaming coupled with nanoparticles

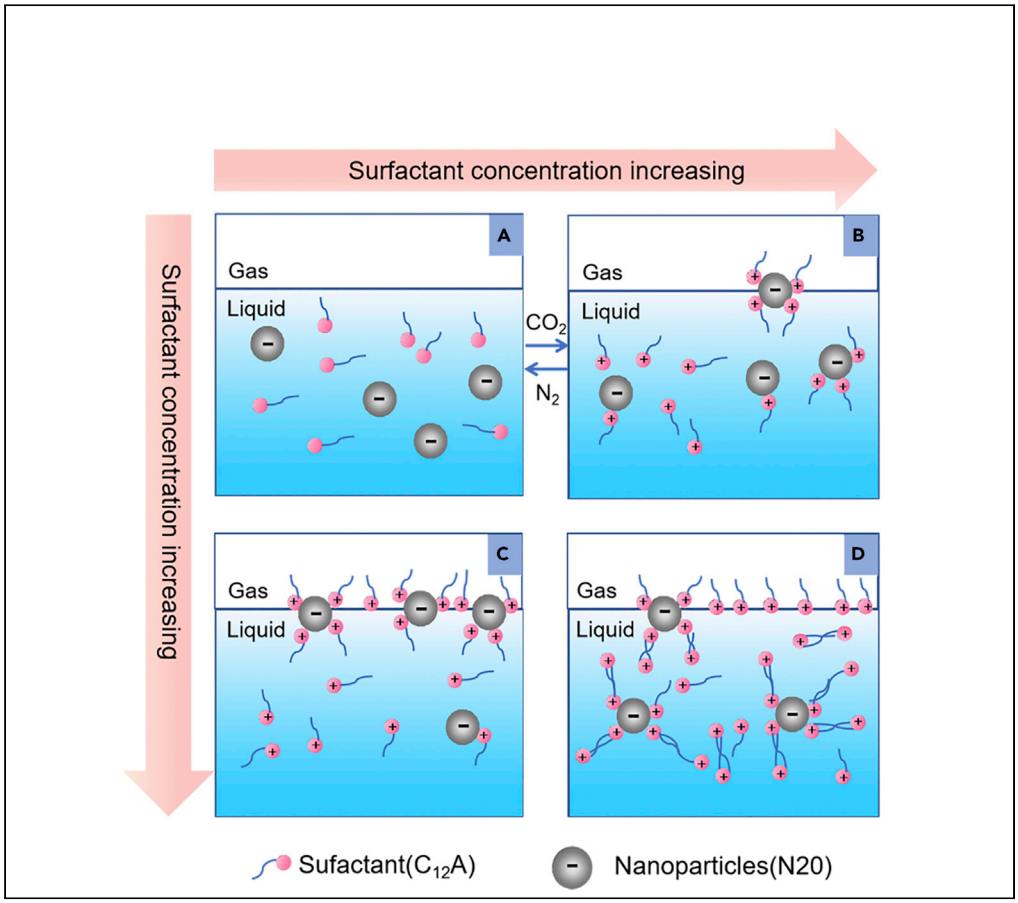

Songyan Li, Shaopeng Li, Kexin Du, Jianzhong Zhu, Liying Shang, Kaiqiang Zhang

lsyupc@163.com (S.L.)
kaiqiang.zhang@pku.edu.cn (K.Z.)

Highlights

Cationic surfactants have the best synergy with NPs with a contact angle of 37.83°

The foam stability increased with the increase of NPs concentration

CO_2/N_2 can control the foaming properties of $C_{12}A$-N20 solution and are reversible

Li et al., iScience 25, 105091
October 21, 2022
https://doi.org/10.1016/j.isci.2022.105091

iScience

CellPress
OPEN ACCESS

Article

Synthesis and stability of switchable CO_2-responsive foaming coupled with nanoparticles

Songyan Li,[1,2,*] Shaopeng Li,[2] Kexin Du,[2] Jianzhong Zhu,[2] Liying Shang,[3] and Kaiqiang Zhang[4,5,6,*]

SUMMARY

CO_2-responsive foaming has been drawing huge attention due to its unique switching characteristics in academic research and industrial practices, whereas its stability remains questionable for further applications. In this paper, a new CO_2-switchable foam was synthesized by adding the preferably selected hydrophilic nanoparticle N20 into the foaming agent $C_{12}A$, through a series of analytical experiments. Overall, the synergy between cationic surfactants and nanoparticles with a contact angle of 37.83° is the best. More specifically, after adding 1.5 wt% N20, the half-life of foam is 14 times longer than that of pure $C_{12}A$ foam. What's more, the $C_{12}A$-N20 solution is validated to own distinctive CO_2-N_2 switching features because very slight foaming degradations are observed in terms of the foaming volume and half-life time even after three cycles of CO_2-N_2 injections. This study is of paramount importance pertaining to future CO_2 foam research and applications in energy and environmental practices.

INTRODUCTION

Foam, a thermodynamically unstable system, consists of a gas dispersed in the liquid phase in the form of small bubbles, where the gas is the dispersed phase and the liquid is the continuous phase (Kruglyakov et al., 2011; Li et al., 2021, 2022a). However, surfactant-stabilized foam is rapidly drained by gravity, resulting in a thinning of the foam lamellar structure and fast foam rupture (Babamahmoudi and Riahi, 2018), which significantly constrains the foam applications in various fields such as detergent (Wolfe et al., 2017), flotation (Bu et al., 2020), energy, and environment (Bai et al., 2018; Sun et al., 2014; Z. Xu et al., 2020a, 2020b).

A more stable foam is usually obtained by increasing the viscosity of the foaming agent solution or adding solid particles. In recent years, nanotechnology has been rapidly developed, and SiO_2 nanoparticles have been synthesized with specific surfaces, which can be well dispersed, adsorbed, etc. Nanoparticles are widely used in materials (Lanasa et al., 2021), medicine (Yadid et al., 2019), oil development fields (Xu et al., 2020a, 2020b), and other fields and have become an important material in some applications with good development prospects. Experimental studies have illustrated that nanoparticles can be adsorbed on the gas–liquid interface to improve the strength of the liquid film, reduce the drainage rate, and inhibit the aggregation of multiphase bubbles (Lv et al., 2020). Moreover, the nanoparticles gathered on the plateau border to form a mesh structure can also increase the stability of the foam. Therefore, it is of great significance to study foams with long-term stability.

However, in addition to the need for a stable foam, it is also necessary to crush the foam rapidly after application. For example, in some oil recovery applications, the foam returns to the surface during CO_2 foam fracturing, and foam sand flushing is difficult to eliminate, which is usually treated by adding defoamers. This method not only increases the cost but also pollutes the environment and makes the foaming fluid unusable (Miller, 2008).

Therefore, it is important to both form a stable foam and deform the foam on demand without changing the composition of the liquid solution. The switchability of foams generated by responsive foaming agents can be controlled by external triggers, including temperature (Chu and Feng, 2011; Davies et al., 2006; Zhang et al., 2013), light (Anwar et al., 2013; Z. Chen et al., 2014b), pH value (Fujii et al., 2005; Huang and Yang,

[1]Key Laboratory of Unconventional Oil & Gas Development (China University of Petroleum (East China)), Ministry of Education, Qingdao 266580, P. R. China

[2]School of Petroleum Engineering, China University of Petroleum (East China), Qingdao 266580, P. R. China

[3]Engineering Technology Branch, CNOOC Energy Development Co., Ltd, Tianjin 300452, P. R. China

[4]Institute of Energy, Peking University, Beijing 100871, P. R. China

[5]Department of Chemical Engineering, Imperial College London, South Kensington Campus, London, SW7 2AZ, UK

[6]Lead contact

*Correspondence: lsyupc@163.com (S.L.), kaiqiang.zhang@pku.edu.cn (K.Z.)

https://doi.org/10.1016/j.isci.2022.105091

2015; Sarker et al., 2017; Tu and Lee, 2014; Yang et al., 2013), magnetic field (Y. Chen et al., 2014a; Lam et al., 2011), redox chemistry (Quesada et al., 2013), or CO_2 (Chai et al., 2014; Chen et al., 2020; Guo and Zhang, 2019; Sun et al., 2019; Yuan et al., 2021).

CO_2 is a nontoxic, inexpensive, and widely available trigger mechanism. Among the many available trigger mechanisms, the CO_2/N_2 trigger is the most environmentally friendly (Chai et al., 2014). The feasible use of CO_2 is an important measure to reduce the impact of greenhouse gases on the environment and can also offset the cost of CO_2 capture. Therefore, CO_2-responsive surfactants have great application potential (Li et al., 2022b). CO_2-responsive surfactants refer to surfactants solute properties that can undergo reversible changes due to introduction and emission of CO_2. Most CO_2-responsive surfactants mainly include amidine, guanidine, imidazole, and tertiary amines (Cunningham and Jessop, 2019). For example, tertiary amine functional groups can undergo protonation reaction with CO_2 to produce cationic bicarbonate, which is unstable. It can be removed from the solution by heating or contacting with inert gases such as N_2 and Ar, so that the cationic bicarbonate can undergo its deprotonation reaction and be reduced to neutral amino group. Jessop et al. (Liu et al., 2006) reported that when CO_2 is injected into aqueous solution, long-chain alkyl amines can undergo protonation reaction to become charged surfactants. When CO_2 was removed with the inert gas Ar at 65°C, charged surfactants were deprotonated and reverted to neutral surfactants. Hao et al. (Xu et al., 2015) used a mixture of organic amine and stearic acid, which controlled foam generation and eliminated foam by alternating CO_2/N_2 injection. Wang et al., 2018 synthesized $UC_{22}AMPM$, which can be protonated in a weakly acidic environment, so CO_2 can be used as a trigger agent. When CO_2 is injected, it can protonate to a cationic surfactant ($UC_{22}AMPM/H^+$); when NH_3/H_2O is injected, it deprotonates back to a neutral tertiary amine. Zhang et al. (Sun et al., 2019) prepared a new CO_2-N_2 switchable surfactant by combining CO_2-responsive surfactant $C_{12}A$ with conventional surfactant SDS. The foam produced by the SDS/$C_{12}A$ surfactant with CO_2 or N_2 as the trigger can be quickly switched between foaming and defoaming. The performance of the SDS/$C_{12}A$ foam was more stable than that of a pure $C_{12}A$ foam.

Currently, the foam produced by commercially available CO_2-responsive surfactants is poorly stabilized, and the stabilizing effect of nanoparticles on foam has been extensively studied. However, there are few studies on whether nanoparticles can cooperate with CO_2-responsive surfactants to stabilize foam. The mechanism of synergistic foam stabilization is not clear. In this study, the optimum ratio of hydrophilic nanoparticles N20 and CO_2-responsive surfactant N, N-dimethyldodecylamine ($C_{12}A$) was experimentally determined. The contact angle of the nanoparticles was optimized. The stability and switchability of $C_{12}A$-N20 foam were investigated, and the synergistic stabilization mechanism of $C_{12}A$-N20 on CO_2 foam was analyzed. The results of this study have broad application prospects for hydrophilic nanoparticles and CO_2-responsive surfactant-stabilized foam.

RESULTS AND DISCUSSION

Preferential selection of SiO_2 nanoparticles

(Figure 1A) depicts the results of foam generation with pure $C_{12}A$. The graph shows that the volume and half-life of the foam first increase and then stabilize with increasing $C_{12}A$ concentration. One of the key factors in the formation of large amounts of foam is surface mobility (Petkova et al., 2020). The low surface mobility ensures that the surfactant can adsorb at the gas–liquid interface for a long enough time and stabilize the liquid film by repulsion when its thickness approaches the critical film thickness h_{CR}. When the concentration of $C_{12}A$ is less than CMC (CMC is defined as the lowest concentration of micelles formed by molecular solution association. The CMC of $C_{12}A$ is 5.01516×10^{-3} mol/L), stable foam cannot be produced under low surfactant coverage (under high surface mobility). In this paper, we measured the CMC of $C_{12}A$ under a CO_2 environment, so it is different from the CMC of $C_{12}A$ in other literature reports (Guo and Zhang, 2019). When the concentration of $C_{12}A$ is greater than CMC, more surfactant molecules are adsorbed on the gas–liquid interface (Lv et al., 2018). The mobility of surfactant molecules at the gas–liquid interface is reduced, and the gas–liquid interfacial tension is also reduced. The adsorption of $C_{12}A$ at the gas–liquid interface also improves the strength and viscoelasticity of the foam film and enhances the stability of the foam. When the $C_{12}A$ concentration reached 0.6 wt %, the volume and half-life of the foam remained essentially unchanged when the $C_{12}A$ concentration was further increased.

To improve the stability of pure $C_{12}A$ foam, eight kinds of hydrophilic SiO_2 nanoparticles were selected as foam stabilizers. The concentrations of SiO_2 nanoparticles were limited to 1.0 wt %. The experimental

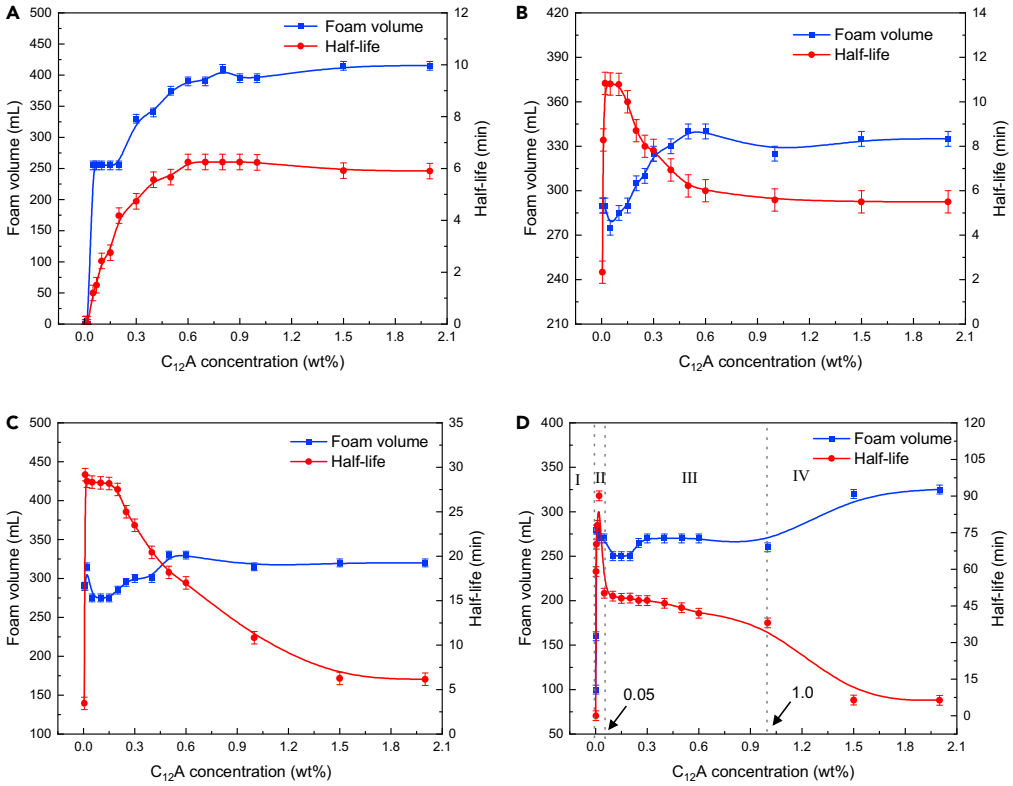

Figure 1. Performance of $C_{12}A$ foam and $C_{12}A$-N20 foam

(A) $C_{12}A$; (B) $C_{12}A$+0.5 wt%N20; (C) $C_{12}A$+1.0 wt%N20; (D) $C_{12}A$+1.5 wt%N20

results are shown in (Figure S1). It can be seen that for the CO_2 foam formed by $C_{12}A$ and eight kinds of SiO_2 nanoparticles, the foam volume and half-life follow the same trends. With increasing $C_{12}A$ concentration, the foam volume first increases and then stabilizes. The half-life of the foam increases first and then decreases, and there is a peak. It can be seen from the (Figure S1) that the nanoparticle aqueous solutions (SG07, WT, PT, and VK-S01A) and $C_{12}A$ have a weak synergistic effect, which may be attributed to the fact that the suspension agent in the nanoparticle aqueous solutions has an adverse effect on foam stability. From our previous study, we know that the contact angle of V15 particles is 51.13°, N20 particles 37.83°, T30 particles 25.12°, and T40 particles 20.12° (Li et al., 2019). Nanoparticles with extreme hydrophilicity would be retained in the liquid phase, and thus were unable to adsorb onto the film and effectively stabilize foam. Similarly, nanoparticles with extreme hydrophobicity would lead to the destruction of the film of foam and were unable to stabilize the foam. This experiment showed that nanoparticles with contact angle of 37.83° have the best synergistic effect with cationic surfactant. At the same time, surfactant adsorption on the surface of nanoparticles can change the contact angle and hydrophobicity of the particles. The optimal surfactant concentration can make the particles have the optimal hydrophobicity and produce the most stable foam.

(Figures 1B–1D) present the foaming volume and half-life of $C_{12}A$-N20 foam when the concentrations of nanoparticles are 0.5, 1.0, and 1.5 wt %. It can be seen from the figure that when the N20 concentration is 0.5 wt %, the synergistic effect is poor, and when the N20 concentration is 1.5 wt %, the synergistic effect is obvious. When 1.5 wt % N20 is added, its half-life is approximately 14 times that of pure $C_{12}A$ foam under the same conditions.

(Figure 1D) can be divided into four regions. In range I, when the concentration of $C_{12}A$ is 0.0025 wt %, the volume of foam is 160 mL, and the $C_{12}A$-N20 solution is not completely foamed. In range II, the half-life of the foam reaches its peak, and the volume of the foam reaches 270 mL. The lower concentration of $C_{12}A$ forms a single adsorption layer on the surface of the SiO_2 nanoparticles. The foam has the largest liquid film mechanical strength and the best foam stability. Because $C_{12}A$ reacts with CO_2 to become a cationic

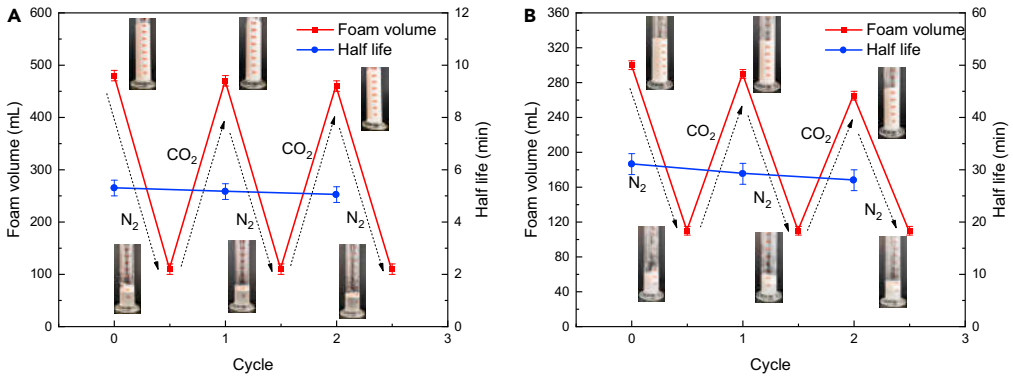

Figure 2. Changes in foam volume and half-life of C_{12}A-N20 solution when CO_2 and N_2 are injected alternately
(A) 0.6 wt% C_{12}A; (B) 0.02 wt% C_{12}A+1.5 wt% N20

surfactant, it adsorbs on the surface of negatively charged SiO_2 nanoparticles through electrostatic interactions. The C_{12}A head group faces the particle surface, and the particle surface changes from strongly hydrophilic to partially hydrophobic. The hydrophobic tail extends in the opposite direction, which also increases hydrophobicity and makes the particles better adsorbed on the gas–liquid interface, hindering the outward diffusion of gas from the foam and increasing the stability of the foam. In range III, the half-life of the foam decreases with increasing C_{12}A concentration due to the hydrophobic association on the carbon chain. The surfactant molecules can be adsorbed on the surface of SiO_2 nanoparticles as a double layer, which changes the wettability of the particles. As the SiO_2 nanoparticles on the gas–liquid interface changes from partly hydrophobic to strongly hydrophilic, the stability of the foams is reduced. In range IV, the volume of the foam is higher, and the half-life is shorter. This is because when the surfactant concentration is high, most of the SiO_2 nanoparticles have a dense double adsorption layer on their surface, which restores strong hydrophilicity so that the particles cannot be stably adsorbed on the gas–liquid interface. At this time, the stability of the C_{12}A-N20 foam is almost the same as that of the C_{12}A foam (Briceño-Ahumada et al., 2021).

Unlike other literature reports where surfactant concentrations much larger than the CMC are required to stabilize the foam, the optimal surfactant concentration of the liquid solution in this paper is only 1/5 of the CMC, which is far lower than the optimal surfactant concentration of the liquid solution in other publications (Kostakis et al., 2006). Trace surfactants may make the surface of nanoparticles active through *in situ* hydrophobicity. When the surfactant concentration approaches or exceeds the CMC, it may create an electric double layer on the surface of the particles, causing the particles to become strongly hydrophilic again and return to the aqueous phase. Considering the foaming volume and the half-life of the CO_2 foam, when the concentration of C_{12}A is in range II and III, the comprehensive performance of the foam at this time is most suitable for the practical application of oilfields.

Stable foams were prepared in which CO_2 was both the initiator phase and the dispersion phase. To provide the generated foam with a switchable function, N_2 is used to close the foam. After injecting CO_2-N_2 into the C_{12}A solution and C_{12}A-N20 solution, the foam volume and half-life changes are shown in (Figure 2). After three cycles, the foaming volume and half-life of the foam only decreased slightly, mainly due to the decrease in surfactant concentration. When CO_2 is injected into the solution, the weakly basic tertiary amino functional group of the amphoteric surfactant molecule C_{12}A in the solution is protonated with the H^+ ionized by carbonic acid so that C_{12}A becomes a cationic surfactant. It adsorbs on the surface of negatively charged SiO_2 nanoparticles by electrostatic interactions, making them hydrophobic *in situ* (Zhang et al., 2016), surface active, and able to generate foam. When N_2 is continuously injected into the solution, CO_2 is expelled from the solution, and the protonated tertiary amine loses its H^+. C_{12}A becomes a nonionic surfactant and separates from the surface of SiO_2 nanoparticles, which eliminates foaming. Therefore, CO_2 plays the dual role of the dispersed phase and the protonated C_{12}A trigger.

After repeated cycles, the foaming ability can still be maintained at a good level, which indicates that the compounded liquid solution has a better effect than the surfactant alone and can be reused. It also indicates that it is "sensitive" to CO_2-N_2. CO_2 is essentially a pH controller, but it has particular advantages

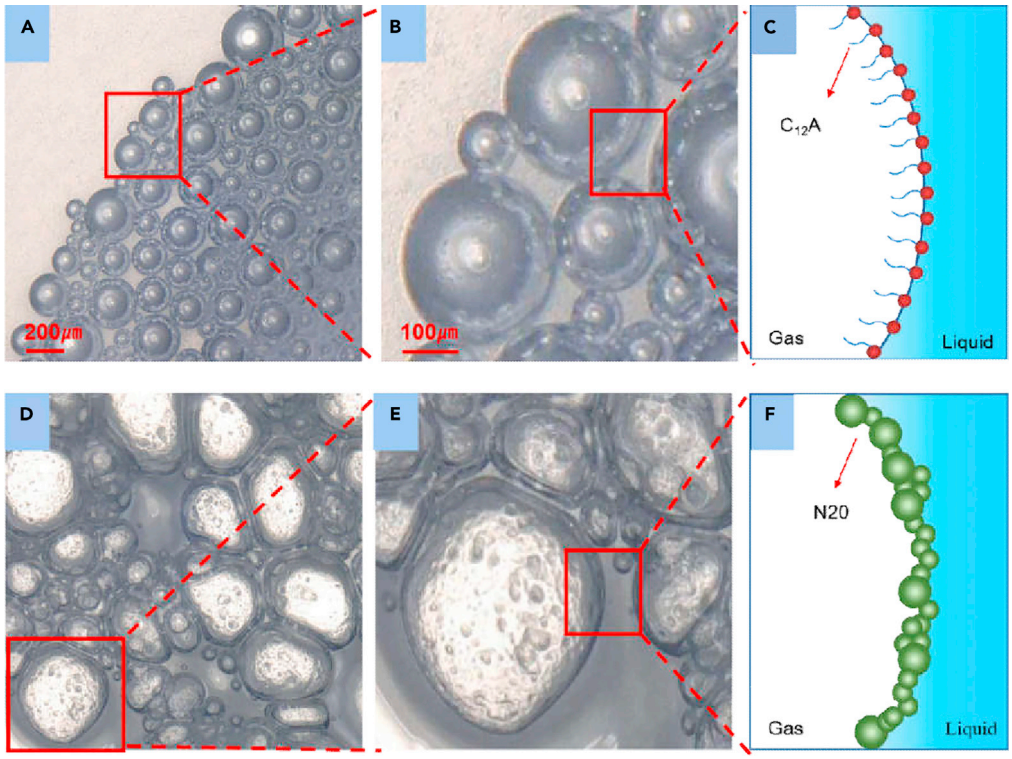

Figure 3. Schematic diagram of the three-dimensional (3D) micrograph structure of the foam under an ultradeep three-dimensional microscope
(A-C) $C_{12}A$; (D-F) $C_{12}A$+1.5 wt%N20.

as a trigger. It successfully avoids contamination and accumulation of solvents and does not produce any byproducts in the liquid solution. The foam developed in this paper can be defoamed by adding N_2 without adding defoamer, which protects the environment and reduces costs. Therefore, it has great application potential in many fields, such as green textiles, soil restoration (Li et al., 2020), enhanced oil recovery (Yekeen et al., 2018), wastewater treatment (Houtz et al., 2018), and mineral flotation (Huang et al., 2018).

Macroscopic characteristics of foams

When SiO_2 nanoparticles are not added, the pure surfactant is adsorbed on the gas–liquid interface. When SiO_2 nanoparticles are added, the surfactant is adsorbed on the surface of the SiO_2 nanoparticles. The adsorption of SiO_2 nanoparticles on the gas–liquid interface improves the viscoelasticity of the foam-liquid film interface, and the mechanical strength of the foam-liquid film framework is increased.

(Figure S2) shows that the excess SiO_2 nanoparticles in the solution flocculate on the plateau boundary of the bubble and form a three-dimensional network (Kostakis et al., 2006), which increases the apparent viscosity of the bubble. At the same time, the particle network can maintain good separation of bubbles, prevent the coalescence of bubbles, hinder the drainage of the liquid film, and make the bubbles more stable. SiO_2 nanoparticles adsorbed on the gas–liquid interface make the liquid film of the foam rough, which increases the flow resistance of the foam and the viscosity of the foam to a certain extent. (Figure S2) shows that the foam viscosity without SiO_2 nanoparticles does not change significantly with increasing surfactant concentration. However, the viscosity of the foam with SiO_2 nanoparticles decreases with increasing surfactant concentration. Excessive surfactant forms a double adsorption layer on the surface of SiO_2 nanoparticles, making the particles strongly hydrophilic again. Only a small number of particles can be adsorbed on the gas–liquid interface, and most of the particles remain in the solution. Therefore, they cannot stabilize the foam, and the viscosity of the foam is reduced.

The structure of the foam and the microscopic changes of the foam over time were recorded using Keene's microscope, as shown in (Figures 3 and 4). From (Figures 3A, 3B, and 3C), it can be seen that the foam

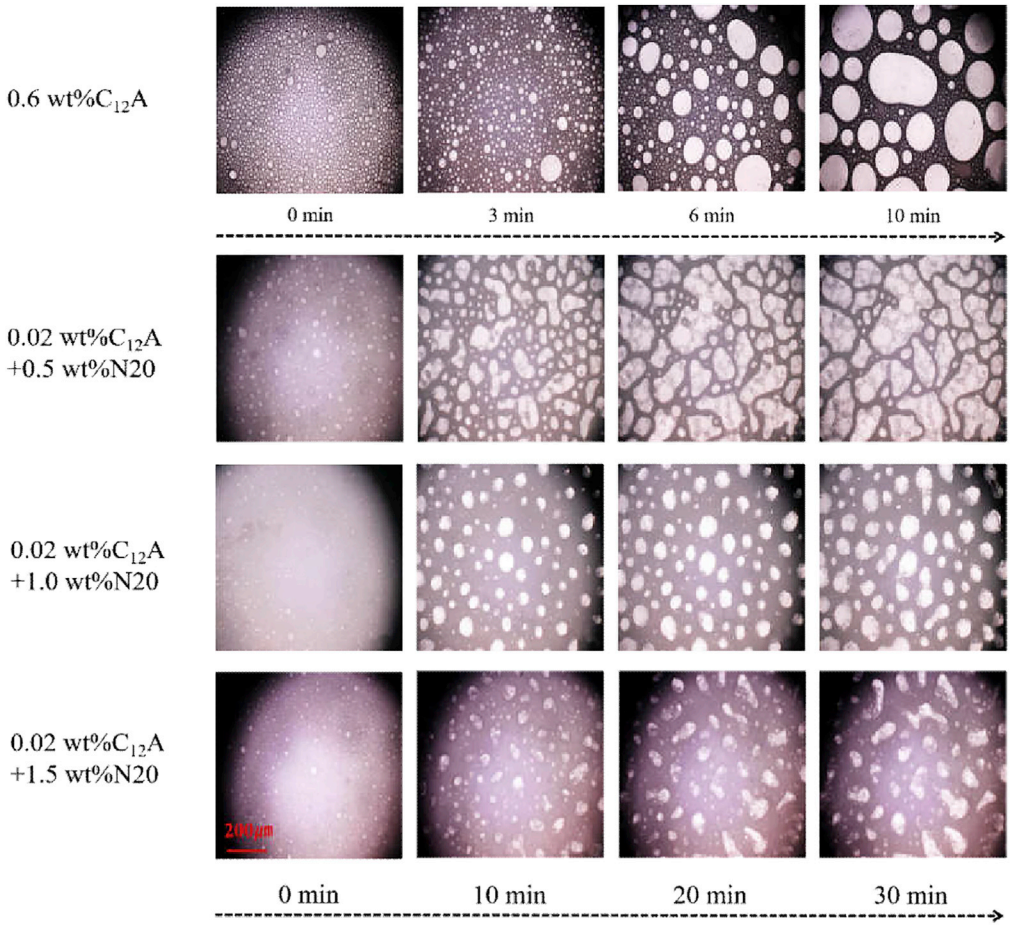

Figure 4. Evolution of the foam structures of $C_{12}A$ and $C_{12}A$-N20 over time under an ultradeep three-dimensional (3D) microscope

formed by $C_{12}A$ has a regular shape, the edges of the foam are smoother, the liquid film of the foam is thinner, and the stability of the foam is relatively poor. When 1.5 wt % N20 was added, the shape of the foam became irregular, and the liquid film of the foam was thicker, as seen in (Figures 3D, 3E, and 3F). SiO_2 nanoparticles are adsorbed on the gas–liquid interface where they produce an uneven enrichment effect, leading to a coarser liquid film in the foam. The adsorption of SiO_2 nanoparticles can increase the mechanical strength of the interface. When enough SiO_2 nanoparticles are adsorbed on the interface, the interface strength is enough to overcome the uniform stretching effect produced by the interfacial tension, so the liquid film cannot be stretched to a smooth state by the interfacial tension. This dense adsorption layer of SiO_2 nanoparticles slows down the agglomeration and disproportionation reactions between bubbles. This reduces the liquid flow between the bubbles and the influence of the outside world on the bubbles.

(Figure 4) depicts the microscopic evolution of CO_2 foam over time. It can be seen from the figure that the shape of the foam formed by $C_{12}A$ is close to a circle, and the stability of the foam is poor. The $C_{12}A$-N20 foam is more irregular and has better foam stability. After adding different concentrations of SiO_2 nanoparticles, the foam morphology can be seen to be very different in approximately 30 min. The size, quantity, and stability of the 1.5 wt % SiO_2 nanoparticles in the field of view is less than that of other foams with stable particle concentrations, which is similar to (Figure 1).

According to the Young-Laplace equation, foams with smaller diameters have a higher pressure, which causes a larger amount of CO_2 to dissolve in the small bubbles. According to Fick's law of diffusion, CO_2 gradually diffuses from bubbles with a smaller diameter through the film to bubbles with a larger

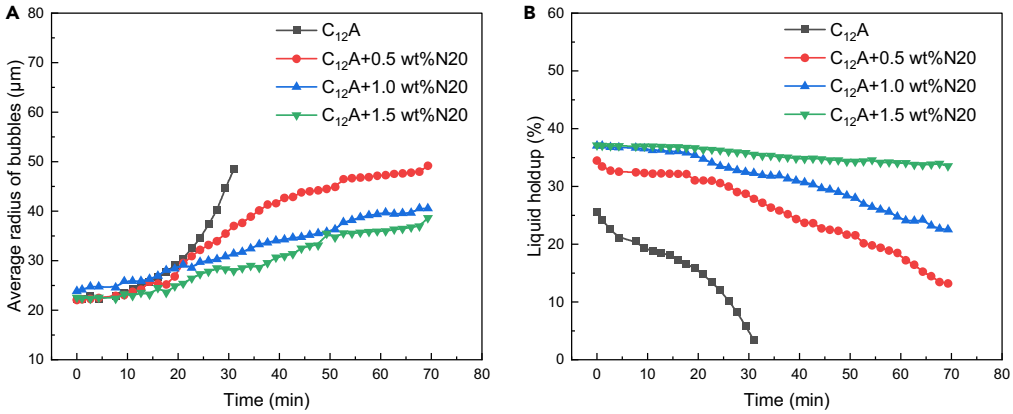

Figure 5. Changes of microstructure of foam with time under different nanoparticle concentrations
(A) average radius of CO2 foam; (B) liquid holdup rate of CO2 foam.

diameter. Small bubbles gradually disappear, and large bubbles become increasingly larger. This process is called Ostwald ripening, which is one of the factors affecting foam stability (Wu et al., 2018). The solubility of CO_2 in water is much greater than that in air or N_2, which increases the Ostwald ripening rate and makes Ostwald ripening very important for CO_2 foams. The images of foam changes with time were recorded using FoamScan, and the images of foams at different times were analyzed by using FoamScan's CSA software. (Figure 5A) depicts optical micrographs of foam evolution. The initial radius of the foam is the same, which is generally approximately 23 μm, and the radius increases significantly with time. After 20 min, the radius of the four foams starts to change, and it can be seen that the radius of the foam decreases with increasing particle concentration at the same time. The foam radius of $C_{12}A$ reached 48.4 μm in 30 min, and the three $C_{12}A$-N20 foams remained very stable, with an average radius of 28.3–37.1 μm. The foam of $C_{12}A$ disappeared at 70 min, but the $C_{12}A$-N20 foam was still very stable, with an average radius of 38.6–49.2 μm. A solid interface is formed on the gas–liquid interface due to the adsorption of SiO_2 nanoparticles. The adsorption of SiO_2 nanoparticles on the gas–liquid interface can greatly reduce the contact area of CO_2 and the liquid film, effectively reducing the diffusion of CO_2, and the Ostwald ripening process is also inhibited. It can be seen that with the increase in nanoparticle concentration, the inhibitory effect becomes more obvious, so SiO_2 nanoparticles can improve foam stability.

(Figure 5B) depicts the variation of the liquid holdup rate of CO_2 foams with time for $C_{12}A$ and $C_{12}A$-N20. The liquid holdup rate was calculated by measuring the total liquid volume, the volume of liquid separated from the foam at different times, and the residual liquid volume by FoamScan. The calculation formula for the liquid holdup rate is presented in Equation 1:

$$f = \frac{V_{tl} - V_{rl}}{V_f} \quad \text{(Equation 1)}$$

where f is the liquid holdup rate, %; V_{tl} is the total volume of the dispersion liquid that generates the foam, mL; V_{rl} is the remaining liquid volume separated from the foam, mL; and V_f is the foam volume, mL.

It can be seen from the figure that the degree of inclination of the straight line indicates the foam drainage speed. For pure $C_{12}A$ foam, the straight-line slope is 59.74°, and the foam drainage speed is fast. The straight-line slope of the $C_{12}A$-N20 foam is 5.688°–30.26°, and the drainage speed slows down considerably. The solid properties of SiO_2 nanoparticles can increase the strength of the liquid film, especially after the liquid film becomes thinner, and its solid skeleton can effectively reduce the possibility of foam rupture and increase the mechanical strength of the foam. At the same time, the presence of SiO_2 nanoparticles in the liquid film in the middle of the gas–liquid interface can also increase the viscosity of the liquid to a certain extent. Thus, this increases the resistance of the liquid from the liquid film to the platform boundary and reduces the thinning rate of the liquid film. This result is consistent with those shown in (Figures 4 and 5).

(Figure 6) is a photograph of the CO_2 foam drainage at different $C_{12}A$ concentrations. It can be seen that (1) is pure $C_{12}A$, and the drainage liquid is clarified. (2)–(8) is a CO_2 foam drainage fluid of $C_{12}A$-N20. As the

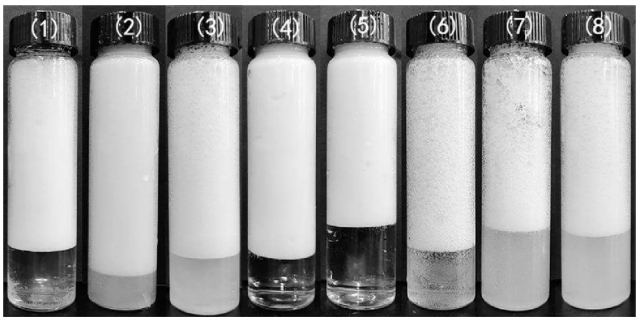

Figure 6. Drainage of foam at different $C_{12}A$ concentrations

concentration of $C_{12}A$ increases, it becomes turbid and then clarified. When the concentration of $C_{12}A$ further increases, the solution becomes turbid again. While SiO_2 nanoparticles have strong hydrophilicity, when the concentration of $C_{12}A$ is relatively low, $C_{12}A$ adsorbs on the SiO_2 nanoparticles, which can make them slightly hydrophobic. Only a small amount of SiO_2 nanoparticles can be adsorbed on the gas–liquid interface, and a large number of particles are retained in the solution, so the drainage liquid is turbid. As the concentration of $C_{12}A$ increases, the surfactant forms a single adsorption layer on the surface of the particle, which can make it more hydrophobic, maximize the contact angle, and stably adsorb on the gas–liquid interface. Therefore, the liquid drainage is clarified, as shown in range II in (Figure 1D). When the concentration of $C_{12}A$ is further increased, additional surfactant adsorption occurs. Through hydrophobic chain-chain interactions, a double adsorption layer is formed, exposing the polar head to the aqueous medium, and the nanoparticles become strongly hydrophilic again. The air or water interface of the foam film is mainly covered by $C_{12}A$, and the nanoparticles are desorbed from the film and returned to the liquid phase, so the drainage liquid is turbid, which is shown in range IV in (Figure 1D). Experiments demonstrate that when the concentration of $C_{12}A$ is low, $C_{12}A$ can form a single adsorption layer on the surface of SiO_2 nanoparticles, which has a strong synergistic effect (Li et al., 2017).

(Figure 7) demonstrates the adsorption state of SiO_2 nanoparticles at the gas–liquid interface with increasing concentrations of $C_{12}A$, which is completely consistent with (Figure 6). When CO_2-N_2 is alternately injected into the solution, $C_{12}A$ can switch between cationic and nonionic states. When CO_2 is injected, $C_{12}A$ becomes a cationic surfactant that can be stably adsorbed on the gas–liquid interface, generating foam related to (1) in (Figure 6). When the solution contains SiO_2 nanoparticles, $C_{12}A$, which becomes a cationic surfactant, is adsorbed on the SiO_2 nanoparticles through electrostatic action, which changes the hydrophilicity and hydrophobicity of the particles. Most of the nanoparticles can be stably adsorbed on the gas–liquid interface. Therefore, the drainage liquid is clarified at this time, which is related to (4–5) in (Figure 6). When the concentration of $C_{12}A$ is further increased, a double adsorption layer forms on the surface of the nanoparticles, which causes the particles to become strongly hydrophilic and return to the solution from the gas–liquid interface. Thus, the drainage solution starts to become turbid in relation to (6–8) in (Figure 6). When CO_2-N_2 is alternately injected into the solution, $C_{12}A$ can adsorb and dissociate from SiO_2 nanoparticles, changing the hydrophobicity of the particles, thus achieving an externally controlled foaming and defoaming process.

Stabilization mechanism of foams

FT-IR spectroscopy is based on the study of radiation absorption and vibration mutation of molecules and polyatomic ions. In addition, the method can examine the molecules attached to the particle surface. To confirm that $C_{12}A$ was adsorbed on SiO_2 nanoparticles, $C_{12}A$-N20 particles were compared with pure N20 particles by FT-IR characterization. It can be seen from (Figure S3) that the absorption band at 2926 cm^{-1} corresponds to the telescopic vibration of -CH_3, and the absorption band at 2855 cm^{-1} corresponds to the telescopic vibration of -CH_2. The detection of N20 particles and $C_{12}A$-N20 particles showed that $C_{12}A$ was successfully adsorbed on the N20 surface.

(Figure S4) demonstrates the interfacial tension between $C_{12}A$-N20 and $C_{12}A$. The interfacial tension of the solution without CO_2 is unchanged with increasing $C_{12}A$ concentration, which proves that pure $C_{12}A$ is not phenotypically active and cannot reduce interfacial tension. In the presence of CO_2, the interfacial tension

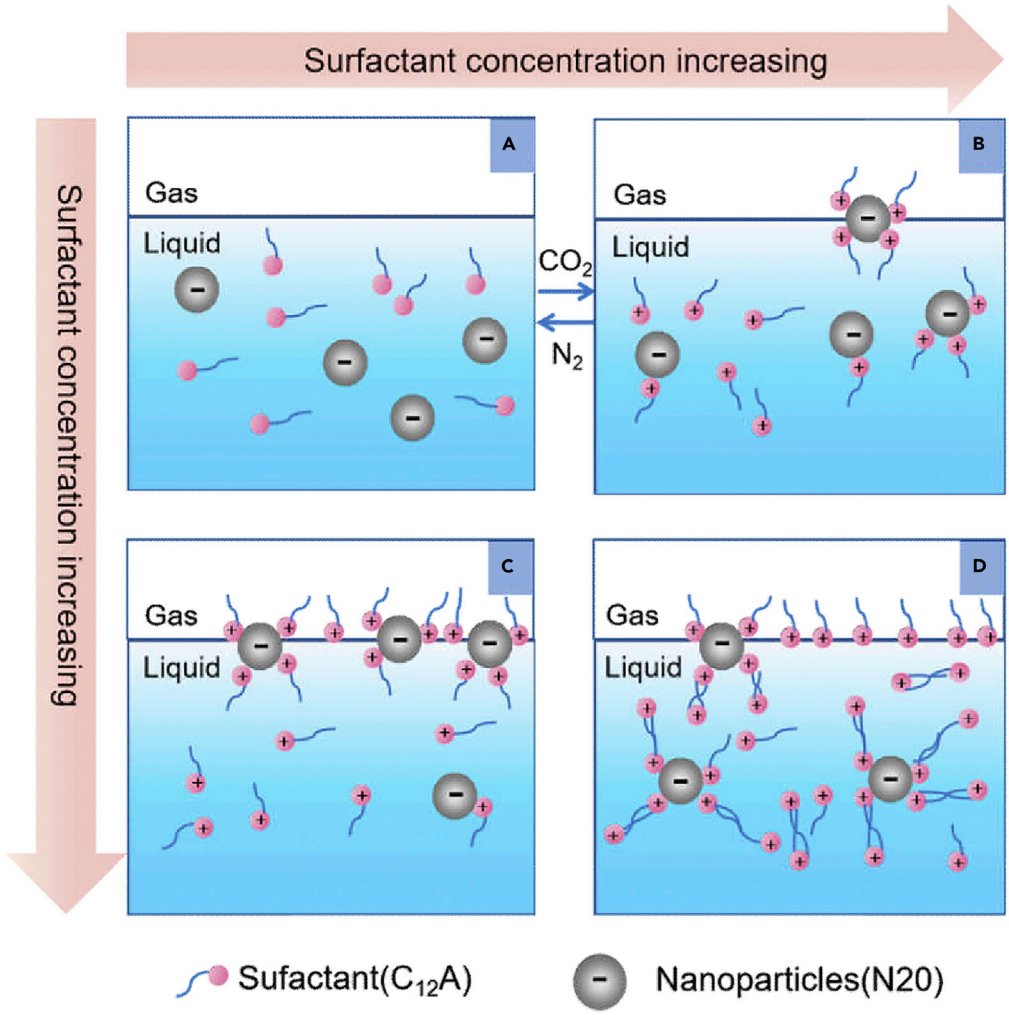

Figure 7. Adsorption state of SiO_2 nanoparticles at the CO_2-water interface as the concentration of $C_{12}A$ increases

(A) low concentration (without CO2); (B) low concentration (with CO2); (C) medium concentration; (D) high concentration.

decreases rapidly with the increase of $C_{12}A$ concentration. When the concentration of $C_{12}A$ is relatively low, the interfacial tension of $C_{12}A$-N20 dispersion is higher than that of $C_{12}A$ solution. $C_{12}A$-N20 dispersion is similar to lotion, in which most nanoparticles remain in the bulk phase rather than at the interface. The surface tension between the dispersion and CO_2 is mainly determined by the surfactant concentration. When the concentration of $C_{12}A$ is greater than that of CMC, the interfacial tension gradually stabilizes. The stable interfacial tensions of $C_{12}A$ and $C_{12}A$-N20 were 24.4 and 23.1 mN/m, respectively. The stable interfacial tension of $C_{12}A$-N20 is lower than that of pure $C_{12}A$. Because more surfactant molecules are adsorbed on the surface of SiO_2 nanoparticles, which can be better adsorbed at the gas–liquid interface than pure surfactant molecules, it allows a denser accumulation of more surfactant molecules at the interface, resulting in a lower interfacial tension (Degen et al., 2011). This effect reduces the gravitation difference between the gas phase and the liquid phase at the interface, thereby reducing the surface tension between the liquid and CO_2 and enhancing the foaming ability and foam stability.

The viscoelastic modulus of the interface is a characterization of the ability of the interface to resist and recover from deformation. A good interfacial viscoelastic modulus helps to improve the resistance of the liquid film to disturbance and to improve the stability of the foam. As shown in (Figure S5), the viscoelastic modulus first increases and then decreases with increasing $C_{12}A$ concentration, reaching a peak at 0.02 wt %. The change in surfactant concentration affects the viscoelastic modulus of the interface

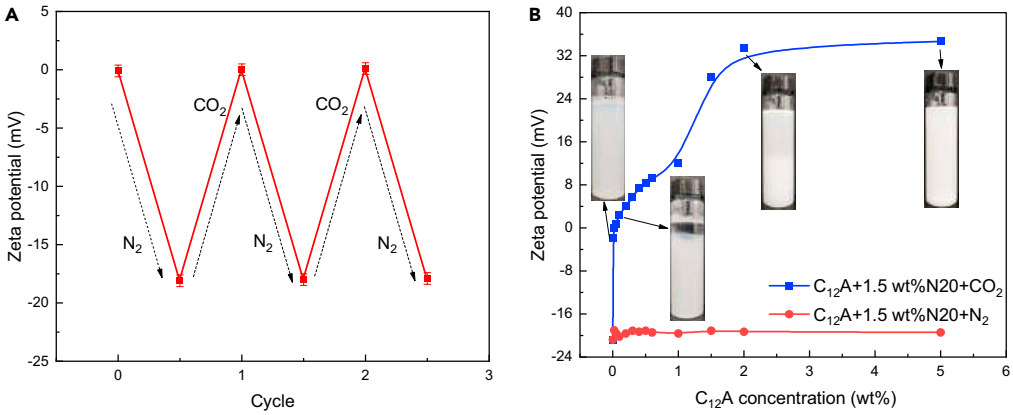

Figure 8. Change of zeta potential of C_{12}A-N20 solution

(A) Changes in the zeta potentials of C_{12}A-N20 solution when alternately injected with CO_2 and N_2;
(B) Effects of C_{12}A concentration on the zeta potential.

from two aspects. On the one hand, it increases the interfacial concentration of surfactant; on the other hand, it increases the ability of surfactant molecules to diffuse from the bulk phase through to the interface. When the surfactant concentration is less than the CMC, the density of the surfactant on the interface changes with the deformation of the interface, which leads to an increase in the interfacial tension gradient. The change in interfacial tension may play a leading role in the increase in the viscoelastic modulus. When the surfactant concentration is higher than the CMC, the surfactant molecules in the bulk phase are replenished to the interface when the interface deforms, reducing the interfacial tension gradient and the expansion pressure gradient of the interface. Interface deformation may play a leading role in the reduction of the viscoelastic modulus. When SiO_2 nanoparticles are added, the viscoelastic modulus of the solution is significantly higher than that of the C_{12}A solution with the same concentration. The adsorption of SiO_2 nanoparticles at the interface causes a curing tendency at the interface, forming a composite film that enhances the mechanical strength of the interfacial layer, which in turn increases the interfacial viscoelastic modulus. At higher surfactant concentrations, the effect of SiO_2 nanoparticles on the viscoelastic modulus disappears. At this point, the particles are covered by a double layer of surfactant molecules and become hydrophilic again. Therefore, when the concentration of C_{12}A is higher, the interface again displays the characteristic properties of a pure surfactant, which corresponds to the previous results in (Figure 1D).

After injecting CO_2-N_2 into the C_{12}A-N20 solution, the zeta potential of the solution changes is shown in (Figure 8A). It was found that the changes of zeta potential of the solution after the passage of CO_2-N_2 were basically consistent with (Figure 2), indicating that the C_{12}A-N20 solution has good reproducibility.

As the concentration of C_{12}A increases, ζ also displays an increasing trend, as shown in (Figure 8B). When C_{12}A is not added, the zeta potential of the SiO_2 nanoparticles in the initial solution is −20.77 mV. As the concentration of C_{12}A increases, the zeta potential of the solution also increases, and when the C_{12}A content is 0.02 wt %, the solution reaches the zero potential point. At this time, the charge on the surface of SiO_2 nanoparticles is completely neutralized by the adsorbed C_{12}A, which forms a single adsorption layer on the surface of the particles, and the hydrophobic interactions between the alkyl chains become obvious. The hydrophobicity of the particles is the strongest, and more particles can be stably adsorbed on the gas–liquid interface, making the foam more stable, which corresponds to range II in (Figure 1D). When the C_{12}A content exceeds 0.1 wt %, the solution begins to stratify, and more flocculation and precipitation appear. The volume or mass of the flocs seems to be proportional to the C_{12}A concentration (Guo and Zhang, 2019). The volume of the flocs plays a vital role in the stability of the foam. The volume of the flocs affects the foaming properties of the solution. Because larger particles are more difficult to adsorb at the gas–liquid interface, the stability of the bubbles is reduced, corresponding to range III in (Figure 1D). When the C_{12}A concentration is greater than 2 wt %, the potential change on the particle surface is small. At this time, the surfactant forms a double adsorption layer on the surface of SiO_2 nanoparticles through the hydrophobic force of carbon chains. This increases the electrostatic repulsion between the particles and makes the aggregated particles redispersed, and the solution becomes stable, corresponding to range IV in (Figure 1D).

Conclusion

It was demonstrated that the CO_2-responsive surfactant $C_{12}A$ and eight types of SiO_2 nanoparticles have a synergistic effect of stabilizing foam, and $C_{12}A$ has the best synergistic effect with SiO_2 nanoparticles N20. Overall, cationic surfactants have the best synergy with nanoparticles with a contact angle of 37.83°. In the solution of 0.02 wt % $C_{12}A$ and 1.5 wt % N20, $C_{12}A$ adsorbs on the nanoparticles by electrostatic interactions, which increases the hydrophobicity of the nanoparticles and enables the particles to adsorb better at the gas–liquid interface. $C_{12}A$ formed a dense single adsorption layer on the nanoparticle surface when the zeta potential was zero. The stability of the foam was best under this condition. The foaming volume of the foam was 270 mL, and the half-life was 90 min, which was 14 times longer than that of the foam produced with $C_{12}A$ alone.

The surface tension of the $C_{12}A$-N20 solution decreases significantly when CO_2 is injected. When the concentration of $C_{12}A$ was increased to 0.2 wt %, the interfacial tension of the $C_{12}A$-N20 solution was 70.55 mN/m in the N_2 environment and decreased to 23.6 mN/m in the CO_2 environment. The foaming performance of the $C_{12}A$ solution and $C_{12}A$-N20 solution can be controlled by using CO_2 and N_2 as switches, and the foaming volume and half-life of the foam only decreased slightly after 3 cycles. This indicates that the solution has good reversibility. The CO_2-responsive surfactant $C_{12}A$ synergistically stabilizes the foam with SiO_2 nanoparticles N20. Nanoparticles adsorbed on the gas–liquid interface can delay Ostwald ripening. Moreover, they can also flocculate on the plateau boundary of the bubble and form a three-dimensional network to slow down the discharge rate.

At 0.02 wt % $C_{12}A$, the nanoparticles increased the interfacial viscoelastic modulus of the foam film from 15.44 mN/m to 30.6 mN/m, which greatly improved the anti-disturbance ability of the liquid film and enhanced the stability of the foam.

Limitations of the study

This work obtained $C_{12}A$-N20 foam, which provided a new strategy for the development and application of nanoparticles stabilized CO_2-responsive foam. However, this study also has limitations. We only discuss that the nanoparticles with a contact angle of 37.83° have the best synergistic effect with cationic surfactant $C_{12}A$, but whether the nanoparticles with a contact angle of 37.83° have such a significant synergistic effect with other cationic surfactants remains to be confirmed. That is, the universality of this strategy is not confirmed. Further relevant research is needed on these aspects.

STAR★METHODS

Detailed methods are provided in the online version of this paper and include the following:

- KEY RESOURCES TABLE
- RESOURCE AVAILABILITY
  - Lead contact
  - Materials availability
  - Data and code availability
- METHOD DETAILS
  - Materials
  - Experimental equipment
  - Experimental procedures
- QUANTIFICATION AND STATISTICAL ANALYSIS

SUPPLEMENTAL INFORMATION

Supplemental information can be found online at https://doi.org/10.1016/j.isci.2022.105091.

ACKNOWLEDGMENTS

This project was financially supported by the National Natural Science Foundation of China (No. 51974346 and No. U20B6003) and the Youth Innovation of University in Shandong Province under (No. 2019KJH002). We are grateful to the Shandong Engineering Research Center for Foam Application in Oil and Gas Field Development and UPC—COSL Joint Laboratory on Heavy Oil Recovery for their assistance with the experimental research.

AUTHOR CONTRIBUTIONS

Conceptualization, S.Y.L. and K.Q.Z.; Methodology, S.Y.L. and S.P.L.; Investigation, S.P.L., J.Z.Z., and K.X.D.; Writing - Original Draft, S.P.L.; Resources, S.Y.L.; Funding Acquisition, S.Y.L.; Supervision, S.Y.L. and K.Q.Z.

DECLARATION OF INTERESTS

The authors declare no competing interests.

Received: March 17, 2022
Revised: June 3, 2022
Accepted: September 1, 2022
Published: October 21, 2022

REFERENCES

Anwar, N., Willms, T., Grimme, B., and Kuehne, A.J.C. (2013). Light-switchable and monodisperse conjugated polymer particles. ACS Macro Lett. *2*, 766–769.

Babamahmoudi, S., and Riahi, S. (2018). Application of nano particle for enhancement of foam stability in the presence of crude oil: experimental investigation. J. Mol. Liq. *264*, 499–509.

Bai, Y., Shang, X., Wang, Z., Zhao, X., and Dong, C. (2018). Experimental investigation of nanolaponite stabilized nitrogen foam for enhanced oil recovery. Energy Fuels *32*, 3163–3175.

Briceño-Ahumada, Z., Soltero-Martínez, J., and Castillo, R. (2021). Aqueous foams and emulsions stabilized by mixtures of silica nanoparticles and surfactants: a state-of-the-art review. Chem. Eng. J. Adv. *7*, 100116.

Bu, X., Wang, X., Zhou, S., Li, B., Zhan, H., and Xie, G. (2020). Discrimination of six flotation kinetic models used in the conventional flotation and carrier flotation of -74 μm coal fines. ACS Omega *5*, 13813–13821.

Chai, M., Zheng, Z., Bao, L., and Qiao, W. (2014). CO_2/N_2 triggered Switchable surfactants with imidazole group. J. Surfactants Deterg. *17*, 383–390.

Chen, A., Chen, J., Wang, D., Xu, J., and Zeng, H. (2020). CO_2/N_2-responsive oil-in-water emulsions using a novel switchable surfactant. J. Colloid Interface Sci. *571*, 134–141.

Chen, Y., Bai, Y., Chen, S., Ju, J., Li, Y., Wang, T., and Wang, Q. (2014a). Stimuli-responsive composite particles as solid-stabilizers for effective oil harvesting. ACS Appl. Mater. Interfaces *6*, 13334–13338.

Chen, Z., Zhou, L., Bing, W., Zhang, Z., Li, Z., Ren, J., and Qu, X. (2014b). Light controlled reversible inversion of nanophosphor-stabilized pickering emulsions for biphasic enantioselective biocatalysis. J. Am. Chem. Soc. *136*, 7498–7504.

Chu, Z., and Feng, Y. (2011). Thermo-switchable surfactant gel. Chem. Commun. *47*, 7191–7193.

Cunningham, M.F., and Jessop, P.G. (2019). Carbon dioxide-switchable polymers: where are the future opportunities? Macromolecules *52*, 6801–6816.

Davies, T.S., Ketner, A.M., and Raghavan, S.R. (2006). Self-assembly of surfactant vesicles that transform into viscoelastic wormlike micelles upon heating. J. Am. Chem. Soc. *128*, 6669–6675.

Degen, P., Wieland, D.C.F., Leick, S., Paulus, M., Rehage, H., and Tolan, M. (2011). Effect of magnetic nanoparticles on the surface rheology of surfactant films at the water surface. Soft Matter *7*, 7655–7662.

Fujii, S., Cai, Y., Weaver, J.V.M., and Armes, S.P. (2005). Syntheses of shell cross-linked micelles using acidic ABC triblock copolymers and their application as pH-responsive particulate emulsifiers. J. Am. Chem. Soc. *127*, 7304–7305.

Guo, S., and Zhang, Y. (2019). CO_2/N_2-switchable high internal phase Pickering emulsion stabilized by silica nanoparticles and low-cost commercial N, N-dimethyl-N-dodecylamine. Colloids Surf. A Physicochem. Eng. Asp. *562*, 119–126.

Houtz, E., Wang, M., and Park, J.S. (2018). Identification and fate of aqueous film forming foam derived per- and polyfluoroalkyl substances in a wastewater treatment plant. Environ. Sci. Technol. *52*, 13212–13221.

Huang, J., and Yang, H. (2015). A pH-switched Pickering emulsion catalytic system: high reaction efficiency and facile catalyst recycling. Chem. Commun. *51*, 7333–7336.

Huang, Z., Cheng, C., Li, L., Guo, Z., He, G., Yu, X., Liu, R., Han, H., Deng, L., and Fu, W. (2018). Morpholine-based gemini surfactant: synthesis and its application for reverse froth flotation of carnallite ore in potassium fertilizer production. J. Agric. Food Chem. *66*, 13126–13132.

Kostakis, T., Ettelaie, R., and Murray, B.S. (2006). Effect of high salt concentrations on the stabilization of bubbles by silica particles. Langmuir *22*, 1273–1280.

Kruglyakov, P.M., Elaneva, S.I., and Vilkova, N.G. (2011). About mechanism of foam stabilization by solid particles. Adv. Colloid Interface Sci. *165*, 108–116.

Lam, S., Blanco, E., Smoukov, S.K., Velikov, K.P., and Velev, O.D. (2011). Magnetically responsive pickering foams. J. Am. Chem. Soc. *133*, 13856–13859.

Lanasa, J.A., Neuman, A., Riggleman, R.A., and Hickey, R.J. (2021). Investigating nanoparticle organization in polymer matrices during reaction-induced phase transitions and material processing. ACS Appl. Mater. Interfaces *13*, 42104–42113.

Li, S., Li, Z., and Wang, P. (2016). Experimental study of the stabilization of CO_2 foam by sodium dodecyl sulfate and hydrophobic nanoparticles. Ind. Eng. Chem. Res. *55*, 1243–1253.

Li, S., Qiao, C., Li, Z., and Wanambwa, S. (2017). Properties of carbon dioxide foam stabilized by hydrophilic nanoparticles and Hexadecyltrimethylammonium bromide. Energy Fuels *31*, 1478–1488.

Li, S., Sun, L., Wang, L., Li, Z., and Zhang, K. (2022a). Hybrid CO_2-N_2 huff-n-puff strategy in unlocking tight oil reservoirs. Fuel *309*, 122198.

Li, S., Wang, L., Su, L., Li, Z., and Zhang, K. (2022b). Carbon dioxide diffusions in Methane-Dissolved pore Fluids: implications for geological carbon storage and utilization in tight formations. Chem. Eng. J. *429*, 132147.

Li, S., Wu, P., and Zhang, K. (2021). Complex foam flow in series and parallel through multiscale porous media: physical model interpretation. Int. J. Heat Mass Transf. *164*, 120628.

Li, S., Yang, K., Li, Z., Zhang, K., and Jia, N. (2019). Properties of CO_2 foam stabilized by hydrophilic nanoparticles and nonionic surfactants. Energy Fuels *33*, 5043–5054.

Li, Y., Hu, J., Liu, H., Zhou, C., and Tian, S. (2020). Electrochemically reversible foam enhanced flushing for PAHs-contaminated soil: stability of surfactant foam, effects of soil factors, and surfactant reversible recovery. Chemosphere *260*, 127645.

Liu, Y., Jessop, P.G., Cunningham, M., Eckert, C.A., and Liotta, C.L. (2006). Switchable surfactants. Science *313*, 958–960.

Lv, Q., Li, Z., Li, B., Husein, M., Li, S., Shi, D., Liu, W., Bai, H., and Sheng, L. (2018). Synergistic mechanism of particulate matter (PM) from coal combustion and saponin from camellia seed

pomace in stabilizing CO_2 foam. Energy Fuels *32*, 3733–3742.

Lv, Q., Zhou, T., Zhang, X., Zuo, B., Dong, Z., and Zhang, J. (2020). Enhanced oil recovery using aqueous CO_2 foam stabilized by particulate matter from coal combustion. Energy Fuel. *34*, 2880–2892.

Miller, C. (2008). Antifoaming in aqueous foams. Curr. Opin. Colloid Interface Sci. *13*, 177–182.

Petkova, B., Tcholakova, S., Chenkova, M., Golemanov, K., Denkov, N., Thorley, D., and Stoyanov, S. (2020). Foamability of aqueous solutions: role of surfactant type and concentration. Adv. Colloid Interface Sci. *276*, 102084.

Quesada, M., Muniesa, C., and Botella, P. (2013). Hybrid PLGA-organosilica nanoparticles with redox-sensitive molecular gates. Chem. Mater. *25*, 2597–2602.

Sarker, M., Tomczak, N., and Lim, S. (2017). Protein nanocage as a pH-switchable pickering emulsifier. ACS Appl. Mater. Interfaces *9*, 11193–11201.

Sun, Q., Li, Z., Li, S., Jiang, L., Wang, J., and Wang, P. (2014). Utilization of surfactant-stabilized foam for enhanced oil recovery by adding nanoparticles. Energy Fuels *28*, 2384–2394.

Sun, S., Zhang, X., Feng, S., Wang, H., Wang, Y., Luo, J., Li, C., and Hu, S. (2019). CO_2/N_2 switchable aqueous foam stabilized by SDS/C_{12}A surfactants: experimental and molecular simulation studies. Chem. Eng. Sci. *209*, 115218.

Tu, F., and Lee, D. (2014). Shape-changing and amphiphilicity-reversing Janus particles with pH-responsive surfactant properties. J. Am. Chem. Soc. *136*, 9999–10006.

Wang, J., Liang, M., Tian, Q., Feng, Y., Yin, H., and Lu, G. (2018). CO_2-switchable foams stabilized by a long-chain viscoelastic surfactant. J. Colloid Interface Sci. *523*, 65–74.

Wolfe, A.J., Hsueh, Y.C., Blanden, A.R., Mohammad, M.M., Pham, B., Thakur, A.K., Loh, S.N., Chen, M., and Movileanu, L. (2017). Interrogating detergent desolvation of nanopore-forming proteins by fluorescence polarization spectroscopy. Anal. Chem. *89*, 8013–8020.

Wu, Y., Fang, S., Zhang, K., Zhao, M., Jiao, B., and Dai, C. (2018). Stability mechanism of nitrogen foam in porous media with silica nanoparticles modified by cationic surfactants. Langmuir *34*, 8015–8023.

Xu, W., Gu, H., Zhu, X., Zhong, Y., Jiang, L., Xu, M., Song, A., and Hao, J. (2015). CO_2-controllable foaming and emulsification properties of the stearic acid soap systems. Langmuir *31*, 5758–5766.

Xu, Z., Cao, A., Chen, L., Cui, S., Yu, G., and Li, Z. (2020a). Flow characteristics of foam in fracture networks. Ind. Eng. Chem. Res. *59*, 19817–19828.

Xu, Z.X., Li, S.Y., Li, B.F., Chen, D.Q., Liu, Z.Y., and Li, Z.M. (2020b). A review of development methods and EOR technologies for carbonate reservoirs. Pet. Sci. *17*, 990–1013.

Yadid, M., Feiner, R., and Dvir, T. (2019). Gold nanoparticle-integrated scaffolds for tissue engineering and regenerative medicine. Nano Lett. *19*, 2198–2206.

Yang, H., Zhou, T., and Zhang, W. (2013). A strategy for separating and recycling solid catalysts based on the pH-triggered pickering-emulsion inversion. Angew. Chem. Int. Ed. Engl. *125*, 7603–7607.

Yekeen, N., Manan, M.A., Idris, A.K., Padmanabhan, E., Junin, R., Samin, A.M., Gbadamosi, A.O., and Oguamah, I. (2018). A comprehensive review of experimental studies of nanoparticles-stabilized foam for enhanced oil recovery. J. Pet. Sci. Eng. *164*, 43–74.

Yuan, C., Chen, D.J., Ye, Q.X., Xiao, K., Hao, L.S., and Nan, Y.Q. (2021). CO_2/N_2-switchable sol–gel transition based on NaDC/NaCl solution: experiments and molecular dynamics simulations. J. Mol. Liq. *325*, 115193.

Zhang, Y., Guo, S., Wu, W., Qin, Z., and Liu, X. (2016). CO_2-Triggered pickering emulsion based on silica nanoparticles and tertiary amine with long hydrophobic tails. Langmuir *32*, 11861–11867.

Zhang, Y., Han, Y., Chu, Z., He, S., Zhang, J., and Feng, Y. (2013). Thermally induced structural transitions from fluids to hydrogels with pH-switchable anionic wormlike micelles. J. Colloid Interface Sci. *394*, 319–328.

STAR★METHODS

KEY RESOURCES TABLE

REAGENT or RESOURCE	SOURCE	IDENTIFIER
Chemicals, peptides, and recombinant proteins		
N,N-dimethyldodecylamine ($C_{12}A$)	Macklin Biochemical Co., Ltd.,	CAS: 112-18-5
SiO_2 nanoparticles (V15, N20, T30, T40)	Wacker Chemical Co., Ltd.,	CAS: 112945-52-5
An aqueous solution of SiO_2 nanoparticles (SG07)	Shanghai Zecheng Co., Ltd.,	CAS: 14808-60-7
An aqueous solution of SiO_2 nanoparticles (WT)	Hangzhou Hege Nanotechnology Co., Ltd.,	CAS: 14808-60-7
An aqueous solution of SiO_2 nanoparticles (PT)	Shanghai Zecheng Co., Ltd.,	CAS: 14808-60-7
An aqueous solution of SiO_2 nanoparticles (VK-S01A)	Xuancheng Jingrui new material Co., Ltd.,	CAS: 14808-60-7

RESOURCE AVAILABILITY

Lead contact

Further information and requests for resources should be directed to and will be fulfilled by the lead contacts, Songyan Li (lsyupc@163.com) and Kaiqiang Zhang (kaiqiang.zhang@pku.edu.cn).

Materials availability

This study did not generate nor use any new or unique reagents.

Data and code availability

- All data reported in this paper will be shared by the lead contact upon request.
- This study did not generate any datasets.
- Any additional information required to reanalyze the data reported in this paper is available from the lead contact on request.

METHOD DETAILS

Materials

For the preparation of CO_2 foam, the surfactant N, N-dimethyldodecylamine ($C_{12}A$) with a purity greater than 98% was purchased from Maclean Industrial Corporation. $C_{12}A$ is the intermediate of the quaternary ammonium salt cationic surfactant, which can be turned into a cationic surfactant after reacting with CO_2. Its relative molecular mass is 213.4 g/mol, and its relative density is 0.787. It appears as a colorless liquid that is soluble in alcohol and insoluble in water. The structure of $C_{12}A$ is presented in Figure S6. CO_2 and N_2 were purchased from Qingdao Tianyuan Gas Company with a purity greater than 99.8%. The distilled water for experiments was produced in the laboratory.

Experimental equipment

In the experiment, a balance (Mettler-Toledo, Switzerland, full scale 120 g, and accuracy 0.001 g) was used to weigh SiO_2 nanoparticles and surfactants. An ultrasonic processor (YP-S17, Hangzhou Success Ultrasonic Equipment Co., Ltd., China) was used to uniformly disperse SiO_2 nanoparticles in water. A high-speed stirrer (Model GJ-3S, Qingdao Senxin, China, stirring speed of 0-15000 r/min) was used to stir the solution to generate foam. An interfacial tension meter (Tracker-H, Teclis, France, full scale 0–200°C and 0.1–20.0 MPa) was used to measure the interfacial tension and viscoelastic modulus of the solutions by the suspension drop method. The viscoelastic modulus of the solution was obtained by changing the volume or area of droplets through sine waves or pulse changes generated by the equipment. An Anton Paar rheometer (Model MCR 302, Anton Paar, Austria, temperature 0–300°C, pressure 0.1–15.0 MPa) was used to measure the viscosity of the foam. A microscope (VHX-5000, Keyence, Japan, 50–5000 times magnification) was used to observe the microstructure of the foam. Fourier transform infrared spectrometer (FT-IR) (Nicolet 6700, Thermo Fisher, USA) was used to measure the FT-IR spectra of SiO_2 before and after the absorption of $C_{12}A$. A Malvern particle size potentiometer (Nano ZS90, Malvern, U.K.) was used to measure the potential

of the solution. FoamScan (Teclis, France, full scale, 20–120°C and 0–8 bar) was used to observe the changes in the shape of the foam at different temperatures over time and to record the changes in the bubble radius and area over time. The foam stability, foam drainage and bubble state evolution at different times and temperatures were observed by the CCD camera of FoamScan. The camera acquired an image every 2 s and could record the image of the foam at the height of one of the four glass prisms throughout the experiment. Through the CSA software of FoamScan, the distribution of the bubble radius and the change in the bubble area over time were obtained. The second CCD camera recorded images of the entire glass column, which determined the total foam volume and foam decay. There were five pairs of electrodes on the rectangular glass column. The first electrode (Helec1 = 20 mm) was used to detect the conductivity of the liquid, and the other four were used to measure the conductivity of the foam. The volume fraction of the liquid in the foam was determined from the conductivity.

Experimental procedures

Preparation and characterization of foams

A certain mass of SiO_2 nanoparticles was added to distilled water to form dispersions with different proportions. All the liquids were dispersed at 30 kHz for 8 min with an ultrasonic processor, left for 3 min, and dispersed again for 8 min, while the temperature of the dispersions was controlled at 25°C with a water bath. Surfactant $C_{12}A$ was added to the dispersion, and then CO_2 was injected into the solution using a stainless-steel needle at a flow rate of 1 L/min at a room temperature of 25°C until the solution reached saturation. The dispersion was left to stand for 12 h at room temperature in a CO_2 environment to stabilize the adsorption of $C_{12}A$ on the surface of SiO_2 nanoparticles. Using the Waring Blender method (Li et al., 2016) with a stirring time of 3 min s at a speed of 8000 r/min, CO_2 was injected into the stirring cup for 1 min to replace the air in it with CO_2, and the mouth of the stirring cup was sealed with cling film to make it froth in the CO_2 environment. The generated foam was quickly transferred to the measuring cylinder. The initial foam volume and the time to drain 50 mL of liquid were recorded as the half-life.

NaCl, $CaCl_2$ and $MgCl_2$ were dissolved in water at a ratio of 8:1:1 to study the effect of salinity on the repeatability of foaming and defoaming. Stable $C_{12}A$ and $C_{12}A$-N20 series solutions with a total salinity value of 1.0×10^5 mg/L were prepared in formation water. The N_2 was sprayed into the bottom of the foam with a stainless-steel needle at a fixed flow rate of 2 L/min, and the defoaming process was recorded. CO_2 was then injected into the defoamed solution at a flow rate of 1 L/min, and the solution was allowed to react thoroughly with CO_2 and then foamed with a high-speed mixer. Foam volume and half-life were recorded for three alternating cycles. All experiments were performed at room temperature (25°C).

Interfacial tension and interfacial viscoelastic modulus

The viscoelastic modulus and interfacial tension of the $C_{12}A$ solution and $C_{12}A$-N20 solution were measured by an interfacial rheometer (Tracker-H). The viscoelastic modulus is a measure of the foam film's ability to resist elastic deformation. For the determination of interfacial tension, a drop of the pendant pear-shaped aqueous solution was prepared using a high-pressure chamber and syringe in a normal temperature and atmospheric pressure CO_2 environment. The droplet profile was recorded using a CCD camera. The interfacial tension of the solution was calculated by the Gauss Laplace equation, and the droplet profile was calculated by Windrop software. The critical micelle concentration (CMC) is an important parameter for each surfactant and affects the surface properties of the surfactant solution, and it can be determined from the interfacial tension. For the determination of the viscoelastic modulus, the oscillation period was 10 s, the oscillation frequency was 0.1 Hz, and the amplitude was 10% of the droplet area. To determine the stable value of the viscoelastic modulus of the solution, a small amplitude of sinusoidal oscillation was applied after no change was observed in the interfacial tension. The average calculated value of the four sinusoidal oscillations was used to calculate the variation in the viscoelastic modulus of the solution at different surfactant concentrations. The calculation formula of the viscoelastic modulus is presented in Equation 2:

$$E = \frac{d\gamma}{d \ln A} \quad \text{(Equation 2)}$$

where E is the interfacial viscoelastic modulus, mN/m; γ is the interfacial tension, mN/m; and A is the area, m^2.

Apparent viscosity of the foams

Apparent viscosity was measured using an Anton Paar rheometer (Model MCR 302). The $C_{12}A$ solution or $C_{12}A$-N20 solution was foamed with a high-speed stirrer according to step 2.3.1, and a small amount of foam was quickly transferred to a measuring cup with the shear rate set at 170 s^{-1}. The temperature was kept at 25°C, and the apparent viscosity and surface shear viscosity of the foam were measured.

Foam microstructure

The microstructure and aggregation of foams were observed at 25°C using an ultradeep field 3D microscope (VHX-5000). Foaming of $C_{12}A$ or $C_{12}A$-N20 solution was conducted with a high-speed stirrer according to step 2.3.1. A small amount of foam was transferred to a clean slide with a glass rod, and the foam was placed as flat as possible on the slide. The focal length and loading stage were adjusted until the image was clear, and the foam liquid film was analyzed by the 3D scanner. Foam performance was measured using the FoamScan. The foam generated by the high-speed stirrer was rapidly transferred into the rectangular foam tube of the FoamScan. The evolution of bubble drainage and bubble state was observed by the CCD camera at different times and temperatures. During the entire experiment, a photo was taken every 2 s to record images of the bubbles. The distribution of the bubble radius and the variation in the bubble area with time were obtained by the CSA software of FoamScan.

Zeta potential

The ζ potential of SiO_2 nanoparticles in $C_{12}A$-N20 solution was determined using a Malvern particle size potentiometer (Zetasizer). A solution of SiO_2 nanoparticles with a concentration of 1.5 wt % was configured and dispersed by an ultrasonic processor for 8 min, and different concentrations of $C_{12}A$ were added. CO_2 was injected to saturation, and the dispersion was left at 25°C with CO_2 for 12 h to reach adsorption equilibrium. The ζ potential was measured three times, and the average value was obtained.

Fourier transform infrared spectroscopy (FT-IR)

The nanoparticles before and after the adsorption of $C_{12}A$ were scanned and analyzed from 4000 cm^{-1} to 400 cm^{-1} using FT-IR spectroscopy. The 1.5 wt % N20 was mixed with 0.02 wt % $C_{12}A$ solution by injecting a sufficient amount of CO_2 and left for 12 h. The solution was then placed in a centrifuge at 6000 r/min and centrifuged for 30 min. The pellet from the centrifugation was dried to constant weight in a CO_2 environment at room temperature. The other part of the experiment used pure N20 as a control.

QUANTIFICATION AND STATISTICAL ANALYSIS

Analyses based on the interfacial tension and viscoelastic modulus of the solution were performed to determine the relationship between interfacial tension and viscoelastic modulus and foam stability. FT-IR and ζ potential analyses of nanoparticles were performed to quantify the effect of $C_{12}A$ on the structure of the nanoparticles.